

DAAI LANGLEY

IN-02  
64860-TM  
P-29

DETAILED NEAR-WAKE FLOWFIELD SURVEYS WITH  
COMPARISON TO AN EULER METHOD OF AN ASPECT RATIO  
4 RECTANGULAR WING

M. D. Klinge\*

North Carolina State University, Raleigh, North Carolina

S. O. Kjelgaard†

NASA Langley Research Center, Hampton, Virginia

and

J. N. Perkins‡

North Carolina State University, Raleigh, North Carolina

(NASA-TM-89357) DETAILED NEAR-WAKE FLOWFIELD SURVEYS WITH COMPARISON TO AN EULER METHOD OF AN ASPECT RATIO 4 RECTANGULAR WING (NASA) 29 F Avail: NTIS EC A01/MF A01 N87-25993 Unclas 0064860 CACL 01A G3/02

\*Research Assistant, Mechanical and Aerospace Engineering, Student Member AIAA

†Research Engineer, Analytical Methods Branch, Member AIAA

‡Professor, Mechanical and Aerospace Engineering, Associate Fellow AIAA

Detailed Near-Wake Flowfield Surveys with Comparison to an  
Euler Method of an Aspect Ratio 4 Rectangular Wing

ABSTRACT

An experimental investigation of the flowfield in the near-wake of an aspect ratio 4 rectangular wing was conducted. This investigation provides a complete detailed set of data for use in the validation of computational methods. An angle of attack of  $8^\circ$  and two Reynolds numbers,  $5.30 \times 10^5$  and  $3.91 \times 10^5$ , were investigated using pitot and six-hole probes. In addition, two types of flow visualization were employed. The data presented includes contours of total pressure, mean velocity, flow angularity, and vorticity distribution data at five chordwise stations of the near-wake ranging from 0.167 to 5.00 chord lengths aft of the trailing edge. The experimental results were compared to the predicted results of a 2-D Euler numerical method.

The results predicted by an Euler method failed to accurately define the flowfield in the region studied in this investigation. Tangential velocities remained relatively constant over the range of  $X/C$  considered though increases in angle of attack and Reynolds number did bring about corresponding increases. Axial velocities also increased with angle of attack and Reynolds number but showed greater sensitivity to increases in  $X/C$ . Graphic displays and contours of the total pressure data indicate that roll-up of the wing tip vortex is essentially complete one and one half chords downstream of the trailing edge.

## INTRODUCTION

The advent of large transport aircraft in the late 1960's and early 1970's introduced a safety risk known as the wake vortex hazard. This hazard has led to Federal Aviation Administration (FAA) regulations requiring up to six nautical miles separation distance between landing aircraft which significantly reduces airport operating capacities and imposes costly delays affecting both airlines and the general public.<sup>1</sup> In order to reduce, if not eliminate, this risk to safety and its subsequent effect on air terminal efficiency, a complete understanding of the complex dynamics of the wake flowfield is necessary. Analysis of the near-wake is an inherent first step towards this understanding. For a more detailed review, an excellent account is presented by Donaldson and Bilanin.<sup>2</sup>

The focus of this research is on the near-wake or roll-up region. Computational methods are progressing toward the prediction of the initial roll-up in the near-wake region. References 3 through 6 offer examples of the techniques employed to numerically calculate vortex wakes. The methods typically involve the solution of the Euler or Navier-Stokes equations using various assumptions concerning the physics of the flowfield to make the solution more tractable. Computational methods require a large number of grid points to adequately model the flow while producing large quantities of information. Consequently, these methods also require great amounts of experimental data with high resolution to compare with the predicted results and validate any assumptions employed in the method.

There are few sets of data furnishing detailed information in the near-wake region of a simple wing geometry. Examples of these are reported in references 6 through 10. This investigation provides one complete detailed set of data for use in the validation of computational methods. The data

presented includes contours of total pressure deficit, total pressure, mean velocity, and vorticity distribution data at five chordwise stations of the near-wake in planes normal to the freestream. The experimental results are compared to the results predicted by the Euler scheme described in reference 5.

The model used for the study was a rectangular wing aspect ratio of four with an NACA 0012 wing section with square tips. The span and chord were 24 and 6 inches respectively. The wing was tested at constant velocities of 166.6 ft/sec and 123.1 ft/sec, corresponding to Reynolds numbers of  $5.30 \times 10^5$  and  $3.91 \times 10^5$  respectively at  $8^\circ$  angle of attack. The effects of the variation of axial distance up to 5 chord lengths downstream of the model's trailing edge, as well as the variation of Reynolds number were investigated.

#### TEST FACILITY

The NACA 0012 wing was tested in the NASA-Langley Basic Aerodynamics Research Tunnel (BART). This facility, is an open return wind tunnel with a test section 28 inches high, 40 inches wide, and 10 feet long. The maximum test section velocity is 220 ft/sec which yields a Reynolds number per foot of 1.4 million. The airflow entering the test section is conditioned by a honeycomb, 4 anti-turbulence screens, and an 11:1 contraction ratio. These flow manipulators, coupled with an excellent speed controller, provide a low-turbulence, uniform flow in the test section. The longitudinal component of turbulence intensity was less than 0.08% over the entire range of tunnel speeds.

The BART Data Acquisition and Control System (DACS) consists of a Hewlett-Packard 9836 desktop computer system which monitors and controls all test instrumentation. Data acquisition software allows entirely automated surveys

of the flowfields behind models of arbitrary geometrical shape. Color displays of the surveyed data are produced by the DACS to allow real-time interpretation of the flowfield.

#### EXPERIMENTAL TECHNIQUE

Two flow visualization techniques, in addition to pitot pressure and six-hole pressure probe measurements, were employed in this study to provide redundant data of specific physical aspects of the near-wake region.

##### Flow Visualization:

The first technique, an oil-type flow visualization using titanium dioxide suspended in kerosene, was employed to determine the existence of any regions of separated flow. The second technique involved using a laser light sheet to determine whether the wing tip vortices shed from the model were in any way effected by the presence of the pitot or six-hole pressure probes. Results from this investigation indicated that the probes inflicted no significant disturbances on the vortex flowfield.

##### Total Pressure Surveys:

Two-dimensional pitot pressure surveys were made in planes normal to the freestream direction at five longitudinal stations with  $X/C = 1.167, 1.500, 2.000, 2.500,$  and  $6.000$ , with respect to the leading edge of the model. The surveys were obtained a half-span at a time due to the limitations of the traversing mechanism. A boundary layer pitot tube was used in this investigation to obtain the total pressures in the near-wake. The tip of the probe was roughly elliptical with a horizontal width of 0.024 inch and a vertical height of 0.013 inch. The wall thickness of the probe was approximately 0.005 inch. The probe was always aligned to the freestream.

A typical flowfield survey consisted of approximately 33 points horizontally by 17 points vertically with a grid point spacing of 0.50 inches. The data acquisition software also allowed for the researcher to specify an "embedded" survey grid in the survey just taken. In this investigation, the embedded grid option was used for more detailed total pressure surveys of the wing tip vortices. These grids usually contained 3500 data points with a grid point spacing of 0.05 inches.

The pitot pressure was measured using an electronic-scanning pressure system equipped with a 1 psid transducer. The transducer was accurate to +0.001 psid. This accuracy was temperature dependent (+0.0005 psid/F); therefore, the data system continuously monitored the upstream air temperature and automatically performed recalibration when the temperature changed 2F. After stepping to each measurement location and pausing 0.5 seconds, the pitot pressure was determined by averaging 255 samples over a one second period. The transducer was referenced to the total pressure just downstream of the last anti-turbulence screen. Hence, the readings provide a measurement of the total pressure deficit found in the near-wake flowfield. This deficit will be large in the cores of the wing tip vortices and near zero in the freestream. Real-time color displays of the flowfield data ensured the absence of lead/lag errors induced by the movement of the probe through the flow in addition to errors resulting from jams in the traversing mechanism.

#### Six-Hole Probe Surveys:

Two-dimensional six-hole probe surveys were made at the same five longitudinal stations mentioned previously. These surveys provided the three components of mean velocity, flow angularity, and the vorticity distributions of the flowfield. The probe was 0.125 inch in diameter with a total pressure port located at the foremost point of a hemispherical tip and a ring of six

interconnected static pressure ports located 1.25 inches aft of the tip. In order to measure the mean velocities and the flow angularity, four additional pressure ports are located approximately  $45^\circ$  to the total port in directions of pitch and yaw<sup>12</sup>. Reference 14 provides a detailed review of the mechanics and calibration of the six-hole probe.

In order to ensure the greatest possible accuracy, the probe was mounted and aligned on the traversing strut using a cathotometer; a telescope with perpendicular cross-hairs which could be rotated to examine roll angle, accurate to  $\pm 3$  minutes. In this way, the probe pitch and yaw ports were within  $0.05^\circ$  of vertical and horizontal respectively. Six-hole probe surveys contained 3402 points in an 81 point by 42 point grid using a grid spacing of 0.20 inches. Embedded surveys were not employed using the six-hole probe. The six-hole probe pressures were measured using the same electronic-scanning system previously mentioned.

At the conclusion of each six-hole probe survey, two freestream points were acquired so that the probe alignment error for each survey could be determined. Reference 14 offers a review of the procedure required to calculate the probe alignment error. Using selected sets of calibration data run through the data reduction process, the accuracy of the probe was determined to be  $\pm 1.0^\circ$  in beta and  $\pm 2.0^\circ$  in alpha.

## RESULTS AND DISCUSSION

The results obtained from the experimental data will be discussed first followed by discussion concerning the comparison of this data to the Euler method of Mitcheltree, et al. (ref. 5). A comprehensive set of data is presented for an angle of attack of  $8^\circ$ .

## Flow Visualization

As already mentioned, two flow visualization methods were employed; the first, a surface flow technique, and the second, a laser light sheet. The important conclusions reached from these investigations were that at an angle of attack of  $8^\circ$  the flow was essentially fully attached to the wing and that the presence of the probes inflicted no significant disturbances on the physical nature of the wake.

## Total Pressure Surveys:

It should be noted that whenever a probe is introduced into a complex flowfield, not only are the probe's measuring characteristics important, but the effect of the probe on the flowfield is equally important and must be considered. Through the laser light sheet flow visualization it was determined that the presence of the probe did not cause any perceptible disturbance to the vortex system. The pitot probe used in this investigation was chosen for its size which allowed for an extremely fine grid pattern as well as offering as little potential disturbance to the flowfield as possible. From the beginning of the study, it was understood that the probe would be incapable of measuring the true total pressure at all locations of the field since it would be aligned to the freestream. Measurements of the total pressure as sensed by the probe versus yaw angle indicate that the probe is insensitive to yaw over a  $\pm 7^\circ$  region with its performance falling off sharply outside this range. The probe had the same sensitivity in pitch as it did in yaw.

Figures 1 through 5 present pressure contours acquired from the total pressure measurements at the five downstream X/C locations at  $8^\circ$ . This series of plots show the development of the wing tip vortex as it travels downstream in the region  $1/6$ th span to either side of the wing tip. The location of the wing tip is represented by (+) in the figures. Very close to the wing's



trailing edge, the actual core of the vortex is still in its developmental stages as the pockets of high pressure deficit surrounding a region of low deficit indicate in figure 1. Furthermore, this figure shows the high pressure gradients that exist in the core close to the wing. The region of low deficit located slightly left of center in the core has measured total pressures very near to that of the freestream. This suggests that, during the initial stages of the roll-up process, portions of the freestream become entrained to the wing tip vortex and are trapped inside the developing core. It is interesting that this phenomenon was not visible in the smoke patterns of the laser light sheet. As the core matures, the pockets of high energy conglomerate and consume the low energy region as shown in figure 2 through 5. In addition, these figures show that the pressure gradients diminish as  $X/C$  increases downstream.

Typical Lexi-data color graphic displays of the  $8^\circ$  case, shown here in black and white, are presented in figures 6 and 7. The total pressure data was divided into twenty bands of color and scaled to enhance the regions of higher pressure deficit. This representation of the pressure losses clearly visualizes the structure of the vortex core and confirms the presence of low deficit regions trapped within the core.

The total pressure deficit data was also employed to help visualize the axial component of the vortex structure. Figures 8 through 12 are plots of the total pressure deficit versus  $Z/b$  taken through the point of maximum deficit. Figure 8 again shows evidence of an undeveloped core. Instead of a single nearly symmetric peak, there exists two regions of almost equal strength. This is consistent with the fact that discrete pockets of high and low pressure deficit are present in the core. The sudden drop in deficit corresponds to the low energy region indicated by figure 1. The maximum

deficit at this first X/C station is -1.00 with a secondary peak at -0.87. Downstream, the core develops into a nearly axisymmetric jet with a peak deficit of only -0.85 as shown in figure 12. The small dip in the deficit values seen below the core is the influence of the sheet of vorticity shed from the wing still wrapping up into the tip vortex. Five chords aft of the trailing edge, its influence is barely visible.

#### Six-Hole Probe Surveys:

The six-hole probe or yaw-pitch probe was used to acquire flow angularity and the mean velocities  $u$ ,  $v$ , and  $w$ . From the mean velocities, vorticity in the plane normal to the freestream was obtained employing the definition

$$\zeta = \frac{dw}{dy} - \frac{dv}{dz}$$

and a second order accurate central differencing numerical scheme. Vorticity contours were acquired in addition to plots of dimensionless tangential and axial velocities versus  $Z/b$ .

Figures 13 through 17 show the variation in dimensionless tangential velocity with distance  $Z/b$ . The maximum rotational velocity achieved for  $\alpha=8^\circ$  was 0.55 at  $X/C=2.0$ . Inside one chord length of the trailing edge, the peak values remained fairly constant at roughly 0.53 before decreasing slightly over the next four chord lengths. These maximums may vary, however, as the resolution of the grid was insufficient to guarantee that all maximums were obtained. Figure 13 represents a case where a peak may have gone undetected.

Non-dimensional axial velocity is plotted in figures 18 through 22. This data is consistent with the total pressure data obtained in that axial velocities within the core are maximum inside of one chord from the trailing edge. Figures 18 and 20 plainly show the axial jet formed by the vortex. In

the core, nearly all velocity exists in the axial direction. Just outside the core, rotational velocities are greatest and a corresponding decrease in axial velocity can be seen to either side of the peak axial component in the two plots just mentioned. Farther downstream (figs. 21 and 22) as viscous effects sap the strength of the jet, the increase in  $U_x/U_\infty$  is far less pronounced. Here too, the grid point spacing was insufficient to detect all the peak axial velocities. As a result, the higher resolution of the total pressure surveys furnish a better view of the axial structure of the vortex core at these downstream locations. It should also be noted that the nondimensional axial velocity is not unity outside the core. This may be attributed to the fact that these quantities were referenced to the tunnel inlet velocity. The same is true for the dimensionless tangential velocity.

From the graphs of non-dimensional tangential and axial velocity, it can be seen at once that at the center of the core the rotational velocity is zero which corresponds closely to the maximum axial velocity. Furthermore, the depressions that flank the peak axial velocities appear to be related to the extremes in tangential velocity. To illustrate this point, figure 23 presents the tangential velocity at  $X/C=1.1667$  with the differential from freestream in axial velocity overlaid. It is clear that some relationship exists between the magnitudes of rotational and axial velocity.

The effect of varied Reynolds number was considered. The model was tested at  $Re=3.91 \times 10^5$ , corresponding to a relatively small 26% drop in Reynolds number. The value for non-dimensional  $U_{\theta \max}$  at  $Re=3.91 \times 10^5$  was approximately  $\pm 0.48$  at both  $X/C=1.167$  and  $2.0$ , which represented a 5.9% decrease. The values of dimensionless  $U_{x \max}$  were roughly 1.1 at  $X/C=1.167$  and 1.15 at an  $X/C$  of  $2.0$  which correspond to drops of 54.5% and 16.7%, respectively. While the tangential velocity drops were consistent, they did not

appear to be significant within the range of the error of this experiment. Though axial velocity losses were more extensive, the limitations concerning the resolution of the grid must be considered as peaks of axial velocity have probably gone undetected. Consequently, it is inconclusive as to whether or not the roll-up process is indeed Reynolds number dependent.

These results did not compare well with those of Chigier and Corsiglia (ref. 7). Several differences exist between the two studies which may account for the discrepancies. The model used in reference 7 was an NACA 0015 rectangular wing with  $AR=5.33$ . The test section Reynolds number and turbulence intensity were not stated in the report but were probably higher than that of this investigation. Finally, the tests in reference 7 were acquired with a three-wire anemometer with the closest X/C station at 10 chords aft of the leading edge, 4 chords more than this study's last station. A true comparison between these results and those of references 6 and 8 was not obtainable as large differences existed in the planforms of the models.

#### Comparison of Experimental Results with Euler Method of Mitcheltree, et al.:

The experimental results of this investigation were compared to the predicted results of the 2-D Euler method developed by Mitcheltree, et al. (ref. 5). The code was run using the same wing geometry while the angle of attack was set to 8. Figures 24 through 28 show the vorticity plots acquired from the experimental and numerical data. It is evident that the two, while similar, are far from identical. The peak vorticities calculated by the Euler code are much larger than those calculated from the experimental data (table 1). While the experimental peaks in vorticity remained fairly constant at about 2.0, the Euler peaks ranged from 5.6 at  $X/C=-1.167$  to 1.6 at  $X/C=6.0$ . It should be noted, however, that the scale of the numerically derived vorticity plot was different in order to accommodate the higher vorticity.

Comparing the tangential velocities revealed a discrepancy of much greater significance. As shown in figures 29-33, the Euler method fails to accurately predict tangential velocities created by the roll-up process. Furthermore, the vorticity contours predicted by the Euler code overestimate the magnitude of vorticity. And finally, obvious problems exist in predicting the location of the roll-up close to the wing and predicting the actual size of the vortex downstream.

#### CONCLUDING REMARKS

An experimental investigation of the flowfield in the near-wake of an aspect ratio 4 rectangular wing has been conducted. This investigation has furnished a complete set of data to be used in the validation of future computational efforts toward the prediction of the near-wake region. The data included pitot pressure and six-hole probe surveys as well as two types of flow visualization.

A comprehensive set of data was acquired at  $Re=5.30 \times 10^5$  and  $\alpha=8^\circ$ . The surveys were made at five longitudinal stations;  $X/C=1.1667, 1.50, 2.00, 2.50,$  and  $6.00$ .

Highly detailed flowfield surveys were obtained in planes normal to the freestream direction. The total pressure and six-hole probe surveys typically included 3400 data points. The sensitivity of the pitot probe was documented as was the accuracy of the six-hole probe. The experimental results were compared to the predicted results of a 2-D Euler method.

The results indicate that both dimensionless tangential and axial velocity are dependent on  $X/C$  location. It was also determined that for conditions of this study, the core was not fully developed within 1.5 chord lengths of the trailing edge. In addition, it was concluded that during the

initial stages of the roll-up process, portions of the freestream became entrained to the wing tip vortex and were trapped inside the developing core.

The comparison to the predicted results of an Euler method indicate that obvious difficulties exist in immediate vicinity of the wing. As a result it seems likely that a Navier-Stokes solver would be better equipped to handle the problems encountered in the prediction of the near-wake.

#### ACKNOWLEDGEMENTS

The authors would like to acknowledge many helpful discussions with Dr. H. A. Hassan, Messrs. W. L. Sellers and R. P. Weston. Their continued guidance and help contributed greatly to the success of this effort.

This research was supported in part by NASA Cooperative Agreement NCCI-84 under the supervision of Dr. Wayne D. Erickson.

## REFERENCES

1. Glessow, Alfred. "Introduction to Symposium on Wake Vortex Minimization," NASA SP-409, 1976.
2. Donaldson, C. duP. and Bilanin, A. J. "Vortex Wakes of Conventional Aircraft," AGARD-AG-204, May 1975.
3. Rossow, V. J. "Inviscid Modeling of Aircraft Trailing Vortices," Symposium on Wake Vortex Minimization, NASA SP-409, 1976.
4. Hoeijmakers, H. W. M. "Computational Vortex Flow Aerodynamics," AGARD-CP-342, 1983.
5. Mitcheltree, R. A., Margason, R. J. and Hassan, H. A. "Euler Equations Analysis of the Initial Roll-Up of Aircraft Vortices," AIAA 86-0078, January 1986.
6. Lee, H. and Schetz, J. A. "Computational and Experimental Study of Tip Vortices," AIAA-83-1886, July 1983.
7. Chigier, N. A. and Corsiglia, V. R. "Wind-Tunnel Studies of Wing Wake Turbulence," Journal of Aircraft, Vol. 9, No. 12, December 1972.
8. El-Ramly, Z. and Rainbird, W. J. "Flow Surveys Behind Wings," AIAA 77-175, January 1977.
9. Hah, C. and Lakshmarayana, B. "Measurement and Prediction of Mean Velocity and Turbulence Structures in the Near-Wake of an Airfoil," Journal of Fluid Mechanics, Vol. 115, pp. 251-282, 1982.
10. Weston, R. P. "Refinement of a Method for Determining Induced and Profile Drag from Detailed Wake Measurements," Ph.D. Dissertation, University of Florida, March 1981.
11. Hammer, J. M. "In-Line Anamorphic Beam Expanders," Applied Optics, Vol. 21, No. 15, p. 2861, August 1982.
12. Fearn, R. L. and Weston, R. P. "Induced Velocity Field of a Jet in a Crossflow," NASA TP-1087, 1977.
13. Kjelgaard, S. O., Sellers, W. L. and Weston, R. P. "The Flowfield Over a 75 Degree Swept Delta Wing at 20.5 Degrees Angle of Attack," AIAA-86-1775, June 1986.
14. Klinge, M. D., "Detailed Near-Wake Flowfield Surveys and Comparison to an Euler Method of an Aspect Ratio 4 Rectangular Wing", M.S. Thesis, N. C. State University, December 1986.

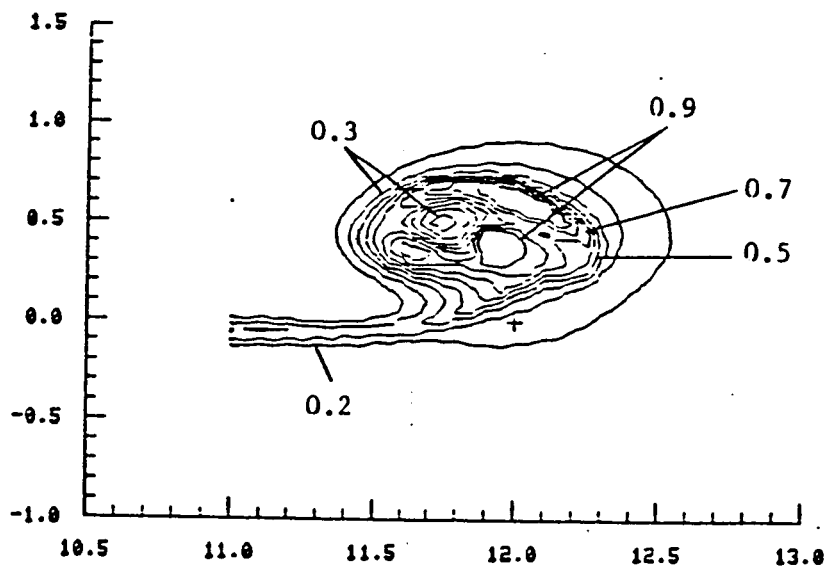


Figure 1 Contour of pressure deficit/ $q$  at  $\alpha = 8^\circ$ ,  
 $X/C = 1.167$ ,  $Re = 5.30 \times 10^5$



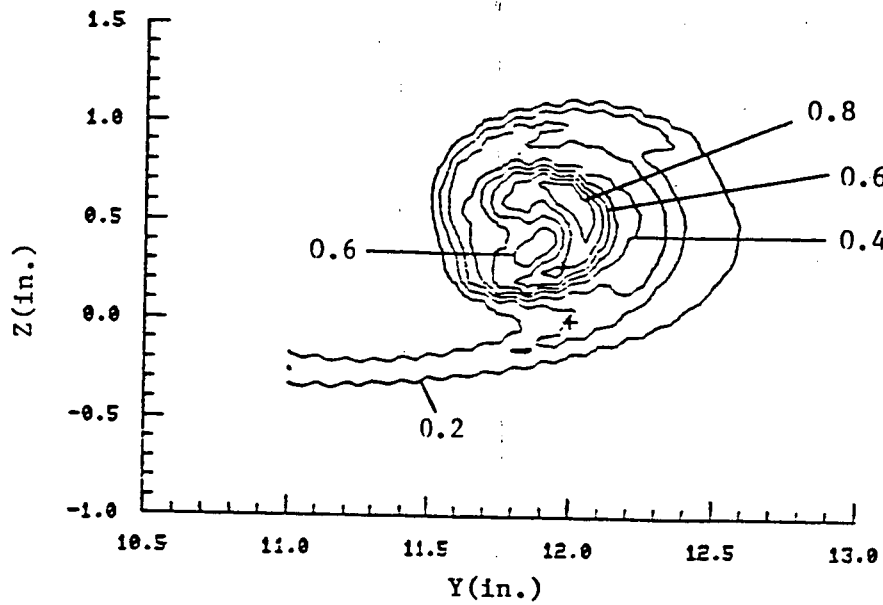


Figure 2 Contour of pressure deficit/ $q$  at  $\alpha = 8^\circ$ ,  
 $X/C = 1.5$ ,  $Re = 5.30 \times 10^5$

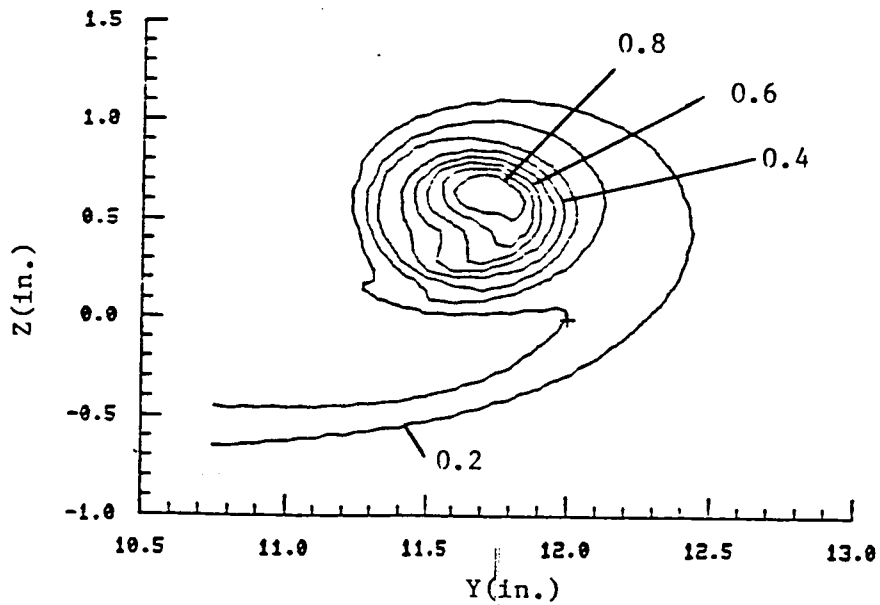


Figure 3 Contour of pressure deficit/ $q$  at  $\alpha = 8^\circ$ ,  
 $X/C = 2$ ,  $Re = 5.30 \times 10^5$

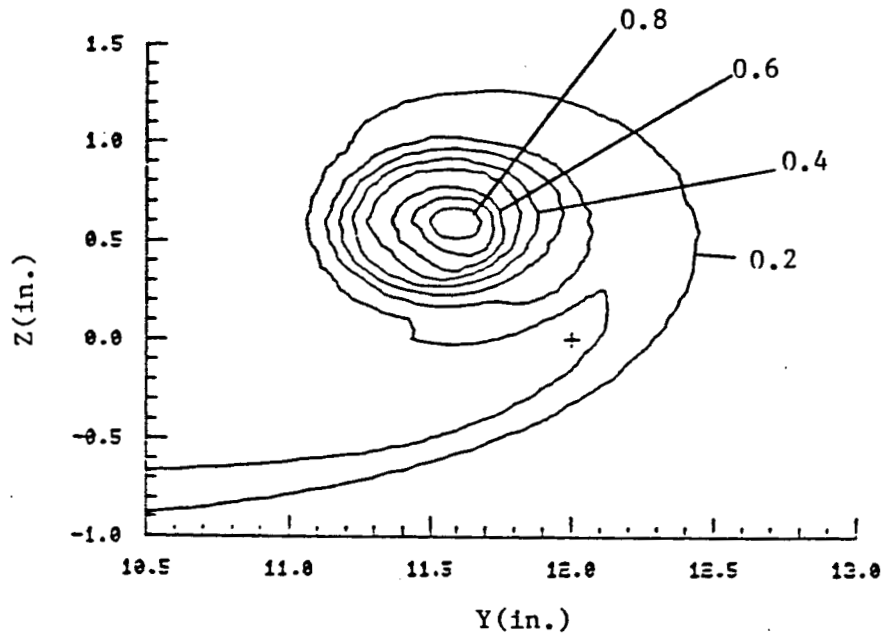


Figure 4 Contour of pressure deficit/ $q$  at  $\alpha = 8^\circ$ ,  
 $X/C = 2.5$ ,  $Re = 5.30 \times 10^5$

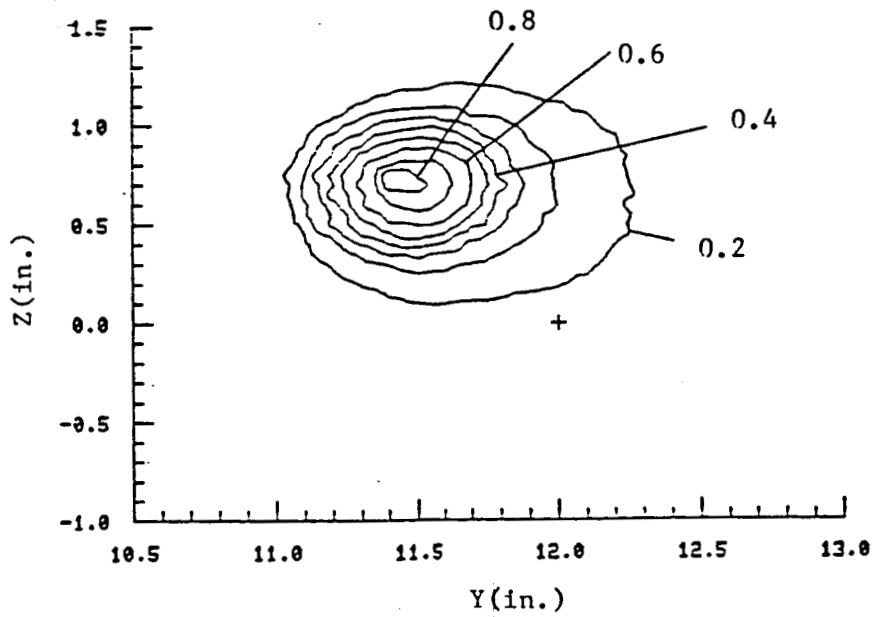


Figure 5 Contour of pressure deficit/ $q$  at  $\alpha = 8^\circ$ ,  
 $X/C = 6$ ,  $Re = 5.30 \times 10^5$

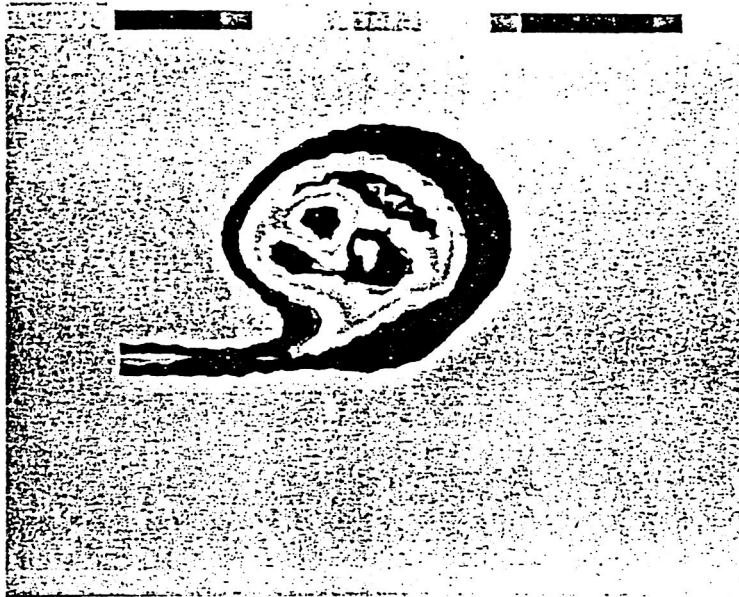


Figure 6 Lexi-data graphic display of total pressure data at  $\alpha_5 = 8^\circ$ ,  $X/C = 1.67$ , and  $Re = 5.30 \times 10^5$

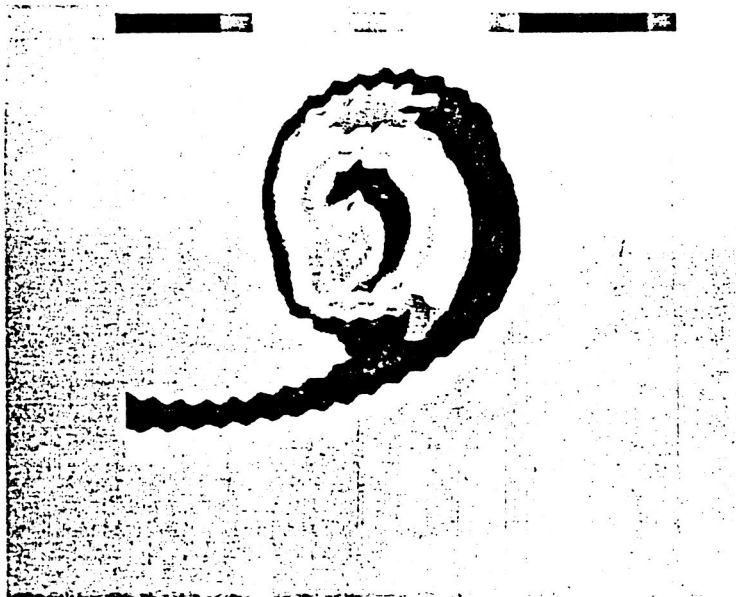


Figure 7 Lexi-data graphic display for total pressure data at  $\alpha = 8^\circ$ ,  $X/C = 1.5$ , and  $Re = 5.30 \times 10^5$

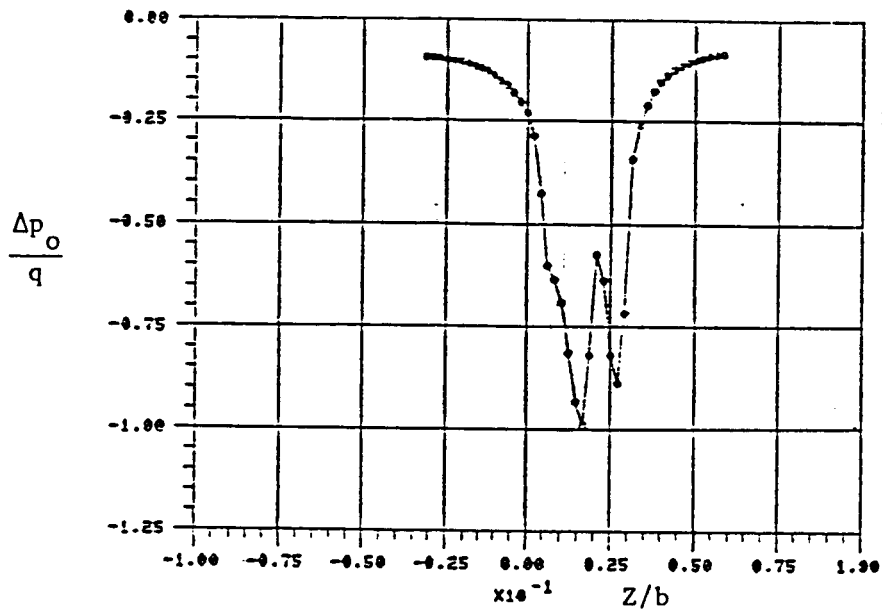


Figure 8 Total pressure deficit axial velocity profile,  $\alpha = 8^\circ$ ,  $X/C = 1.167$ ,  $Re = 5.30 \times 10^5$

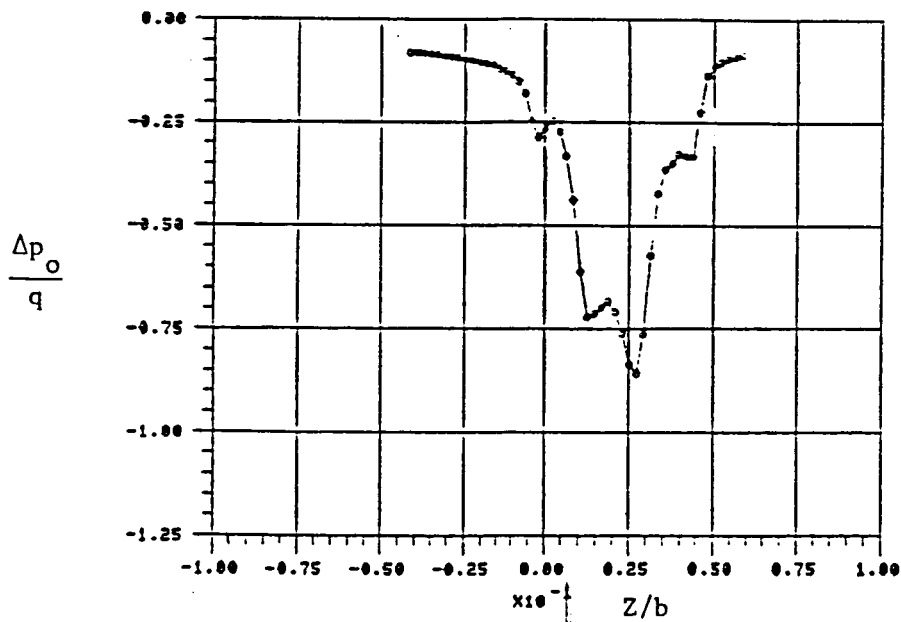


Figure 9 Total pressure deficit axial velocity profile,  $\alpha = 8^\circ$ ,  $X/C = 1.5$ ,  $Re = 5.30 \times 10^5$

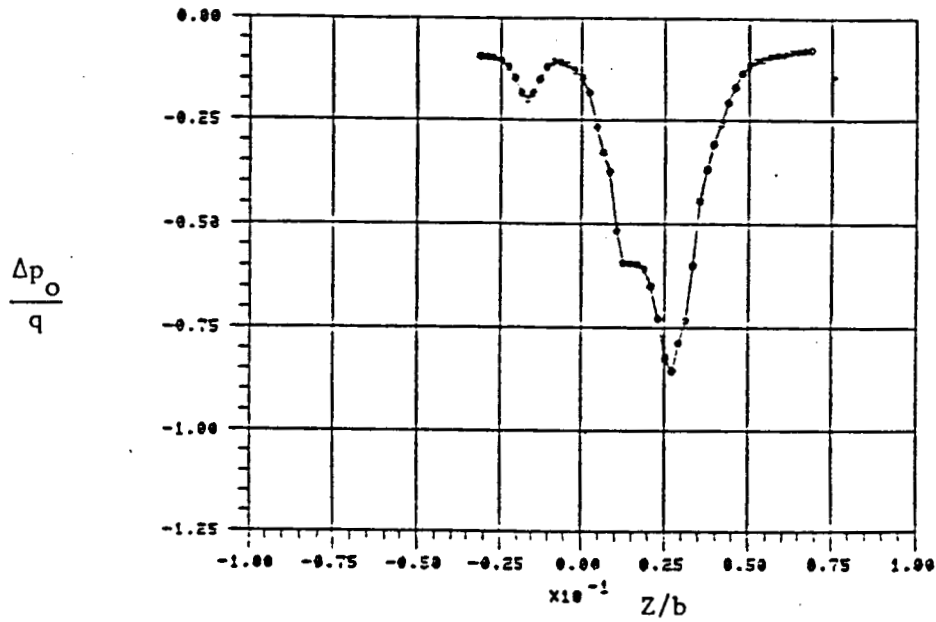


Figure 10 Total pressure deficit axial velocity profile,  $\alpha = 8^{\circ}$ ,  $X/C = 2.0$ ,  $Re = 5.30 \times 10^5$

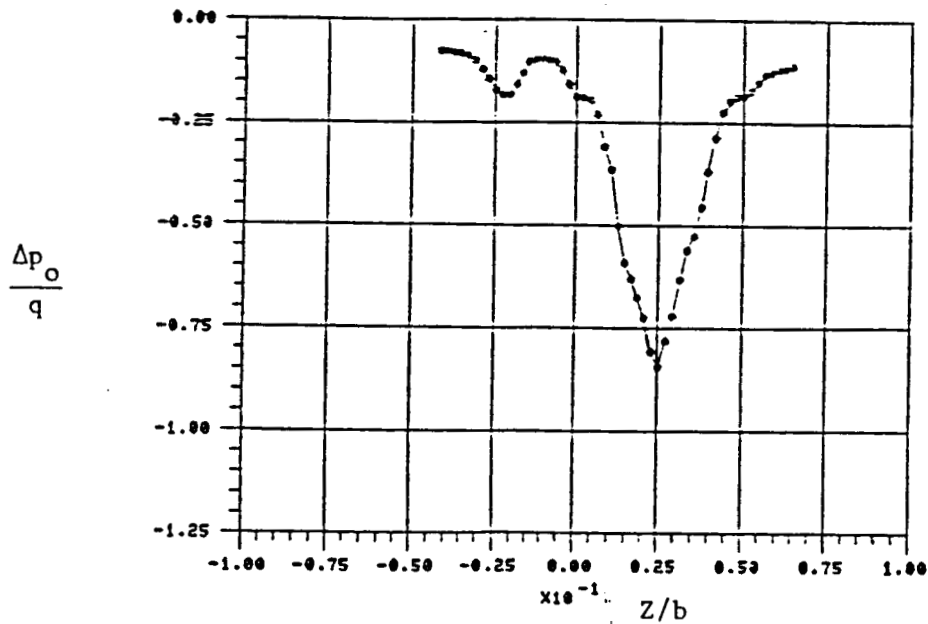


Figure 11 Total pressure deficit axial velocity profile,  $\alpha = 8^{\circ}$ ,  $X/C = 2.5$ ,  $Re = 5.30 \times 10^5$

ORIGINAL PAGE IS  
OF POOR QUALITY

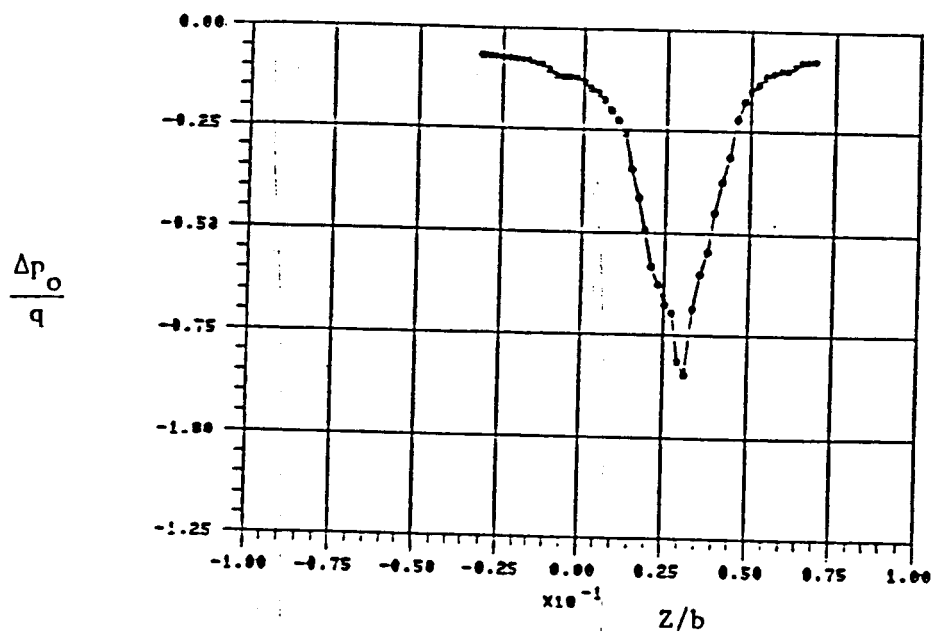


Figure 12 Total pressure deficit axial velocity profile,  $\alpha = 8^\circ$ ,  $X/C = 6.0$ ,  $Re = 5.30 \times 10^5$

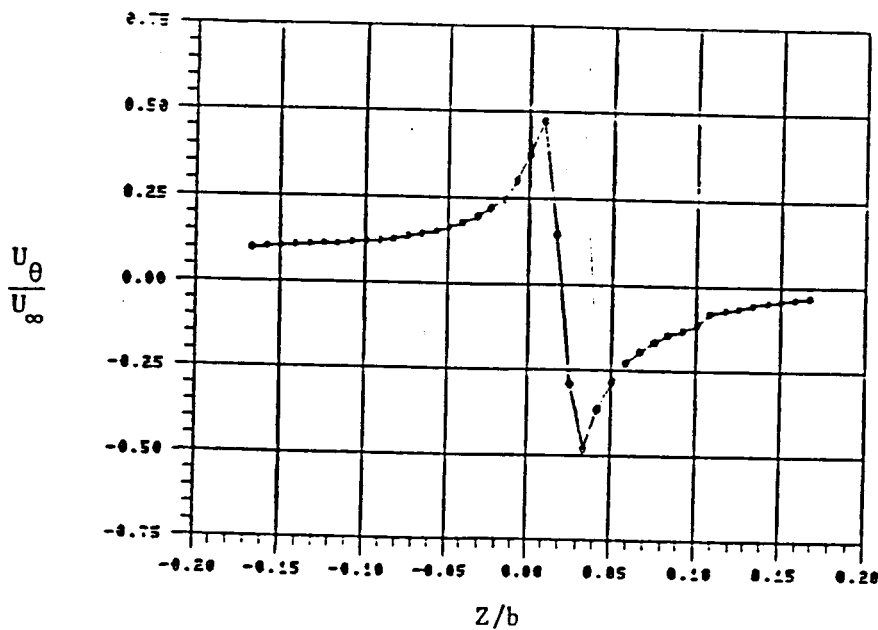


Figure 13 Tangential velocity profile,  $\alpha = 8^\circ$ ,  $X/C = 1.167$ ,  $Re = 3.91 \times 10^5$

ORIGINAL PAGE IS  
OF POOR QUALITY

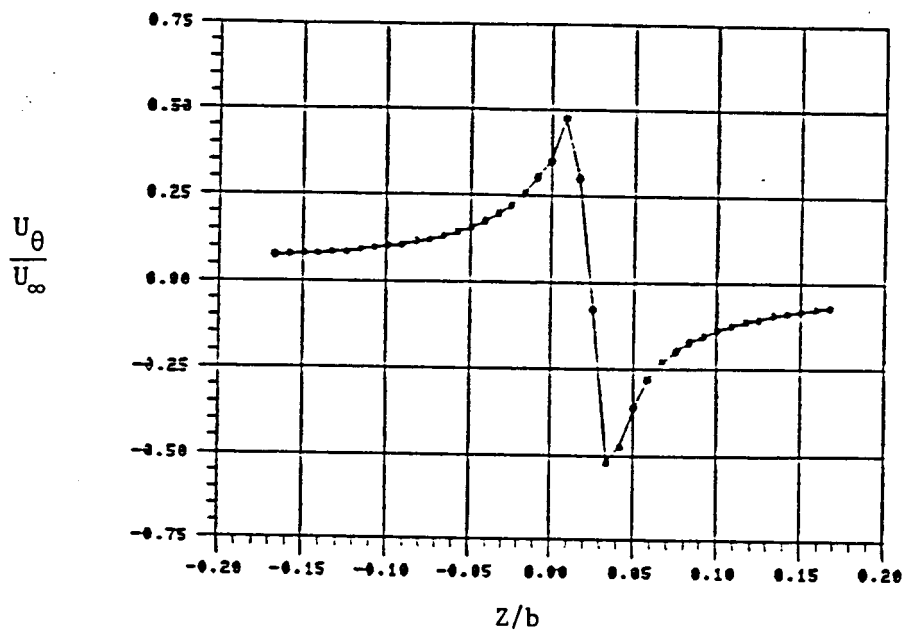


Figure 14 Tangential velocity profile,  
 $\alpha = 8^\circ$ ,  $X/C = 1.5$ ,  
 $Re = 5.30 \times 10^5$

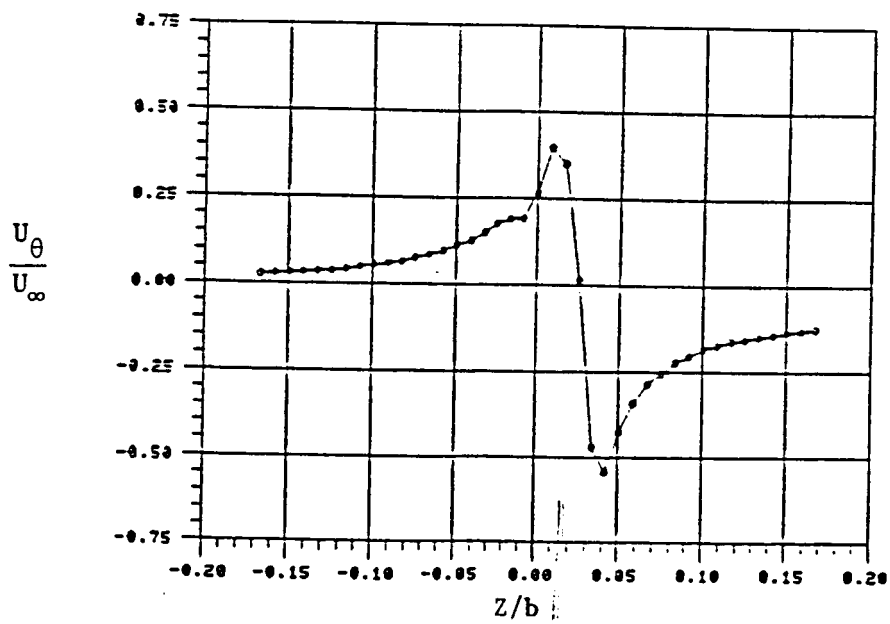


Figure 15 Tangential velocity profile,  
 $\alpha = 8^\circ$ ,  $X/C = 2.0$ ,  
 $Re = 5.30 \times 10^5$

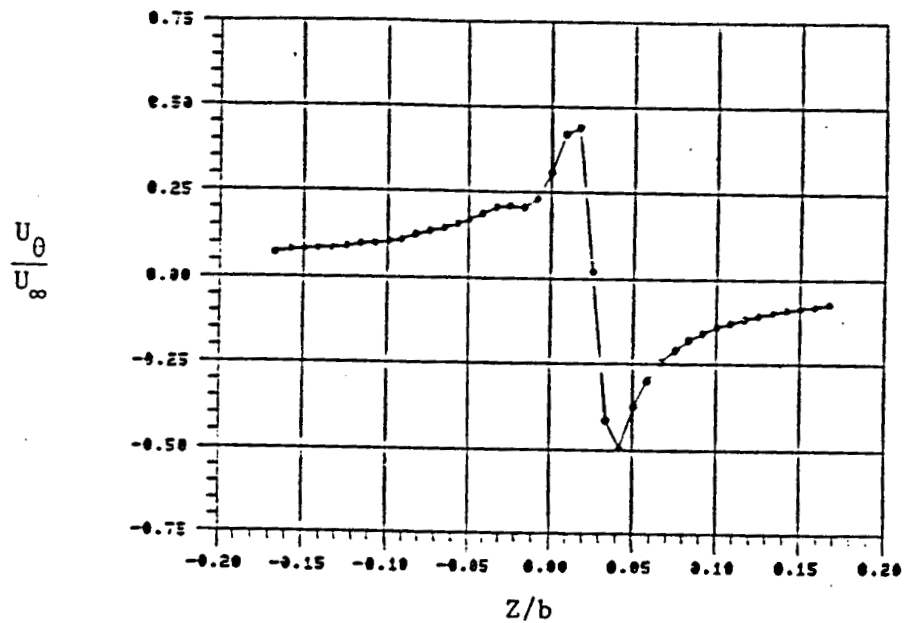


Figure 16 Tangential velocity profile,  
 $\alpha = 8^\circ$ ,  $X/C = 2.5$ ,  
 $Re = 5.30 \times 10^5$

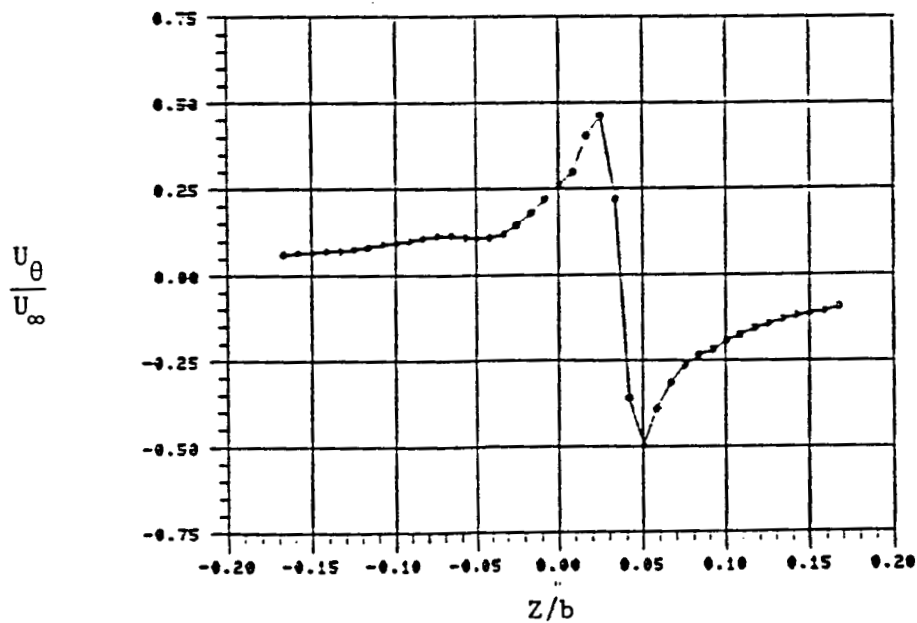


Figure 17 Tangential velocity profile,  
 $\alpha = 8^\circ$ ,  $X/C = 6.0$ ,  
 $Re = 5.30 \times 10^5$



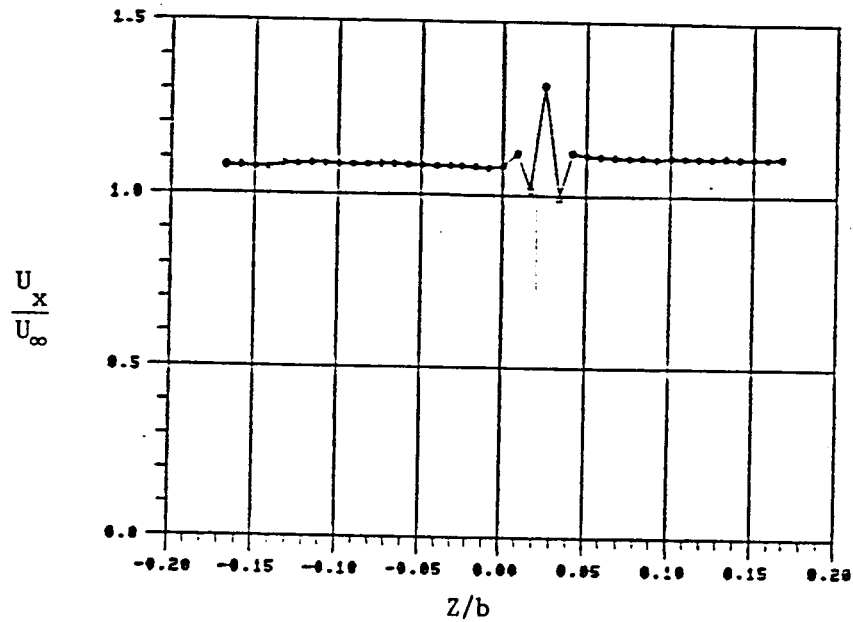


Figure 18 Axial velocity profile,  
 $\alpha = 8^\circ$ ,  $X/C = 1.167$ ,  
 $Re = 5.30 \times 10^5$

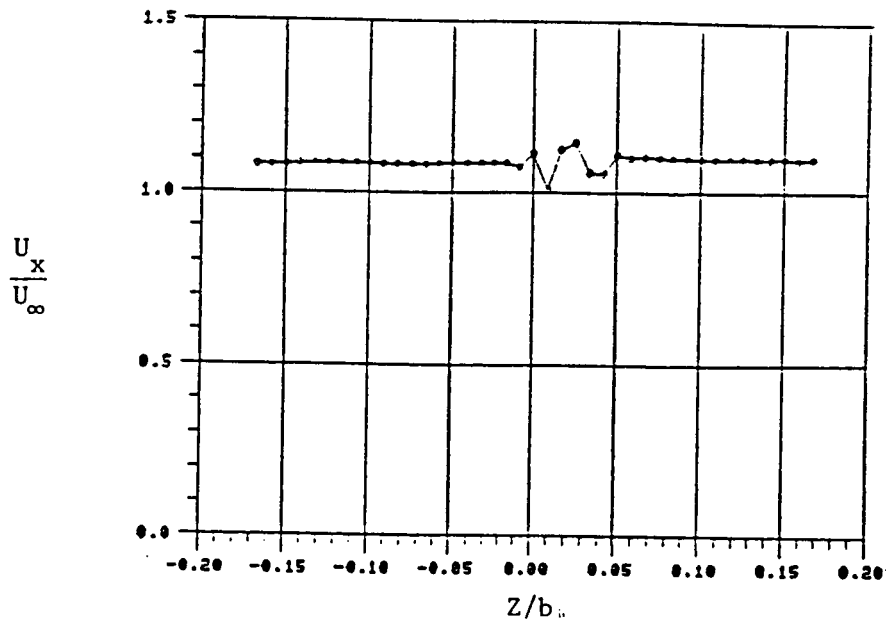


Figure 19 Axial velocity profile,  
 $\alpha = 8^\circ$ ,  $X/C = 1.5$ ,  
 $Re = 5.30 \times 10^5$

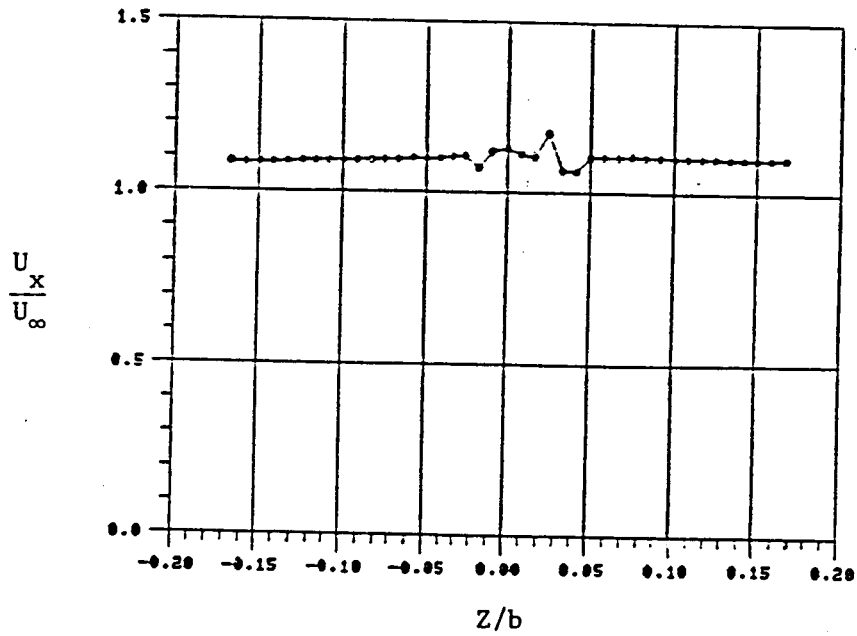


Figure 20 Axial velocity profile,  
 $\alpha = 8^\circ$ ,  $X/C = 2.0$ ,  
 $Re = 5.30 \times 10^5$

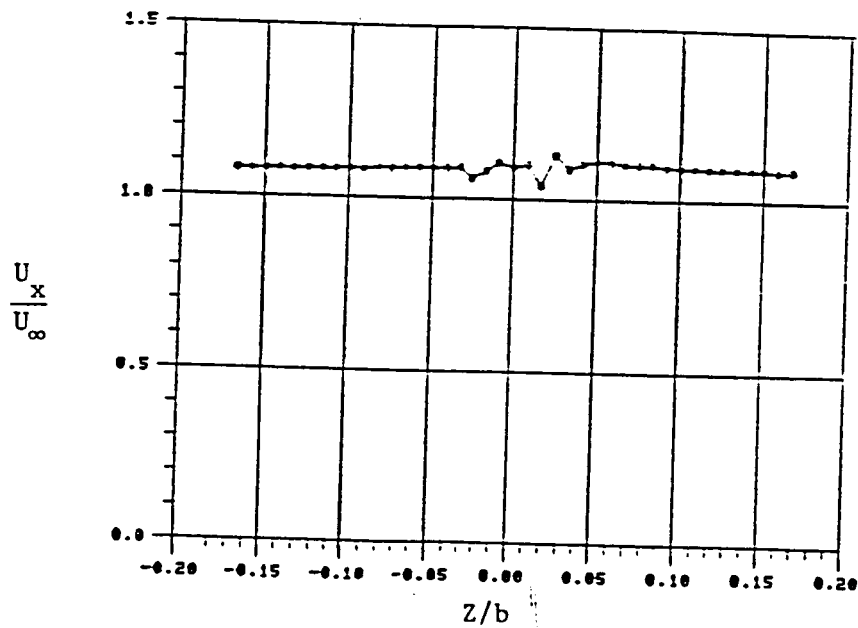


Figure 21 Axial velocity profile,  
 $\alpha = 8^\circ$ ,  $X/C = 2.5$ ,  
 $Re = 5.30 \times 10^5$

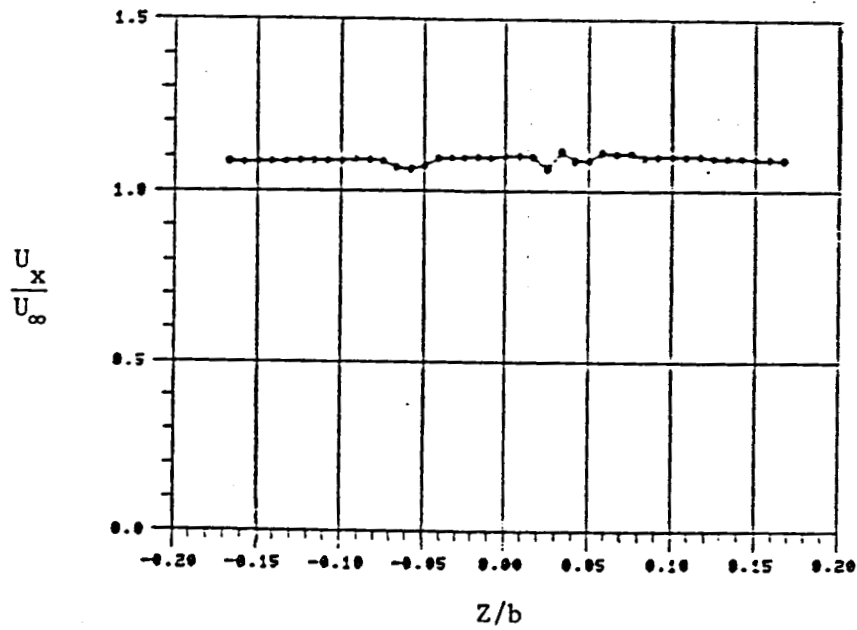


Figure 22 Axial velocity profile,  
 $\alpha = 8^\circ$ ,  $X/C = 6.0$ ,  
 $Re = 5.30 \times 10^5$

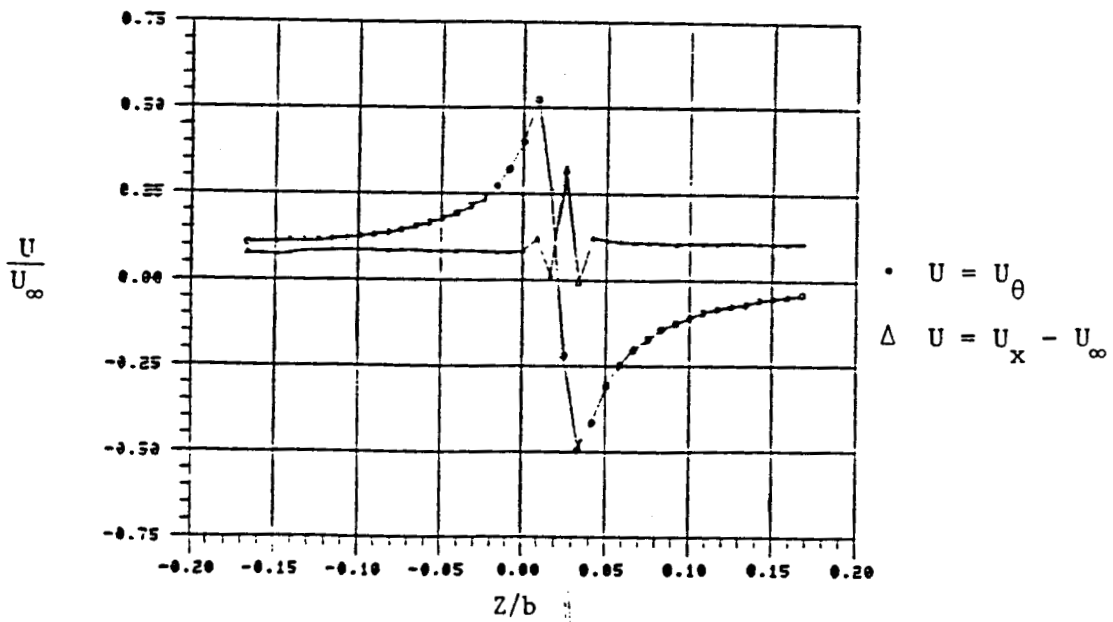


Figure 23 Comparison of axial velocity differential  
to tangential velocity profile,  $\alpha = 8^\circ$ ,  
 $X/C = 1.167$ ,  $Re = 5.30 \times 10^5$

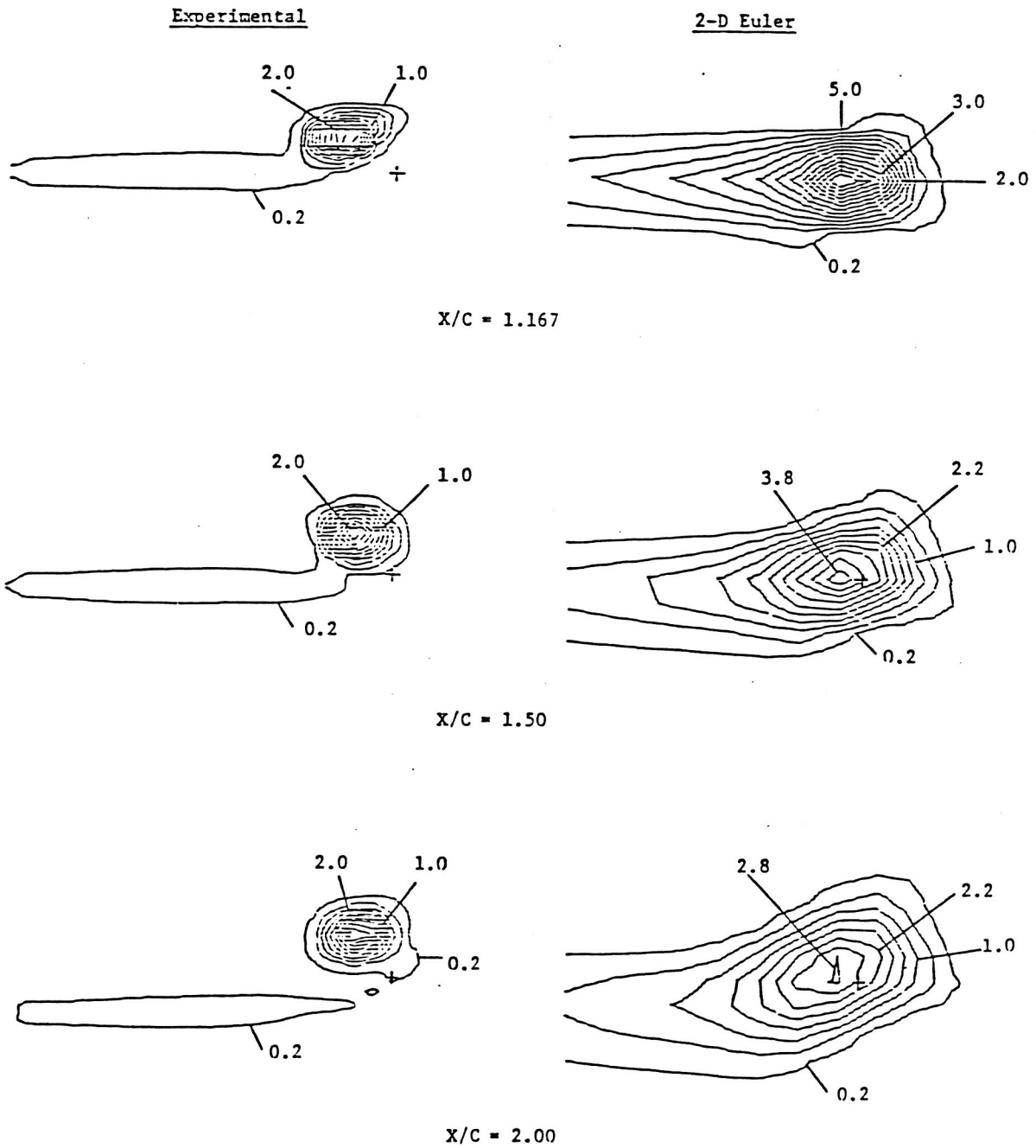


Figure 24 Comparison of vorticity contours to 2-D Euler Method  
 $(\alpha = 8^\circ, Re = 5.30 \times 10^5)$

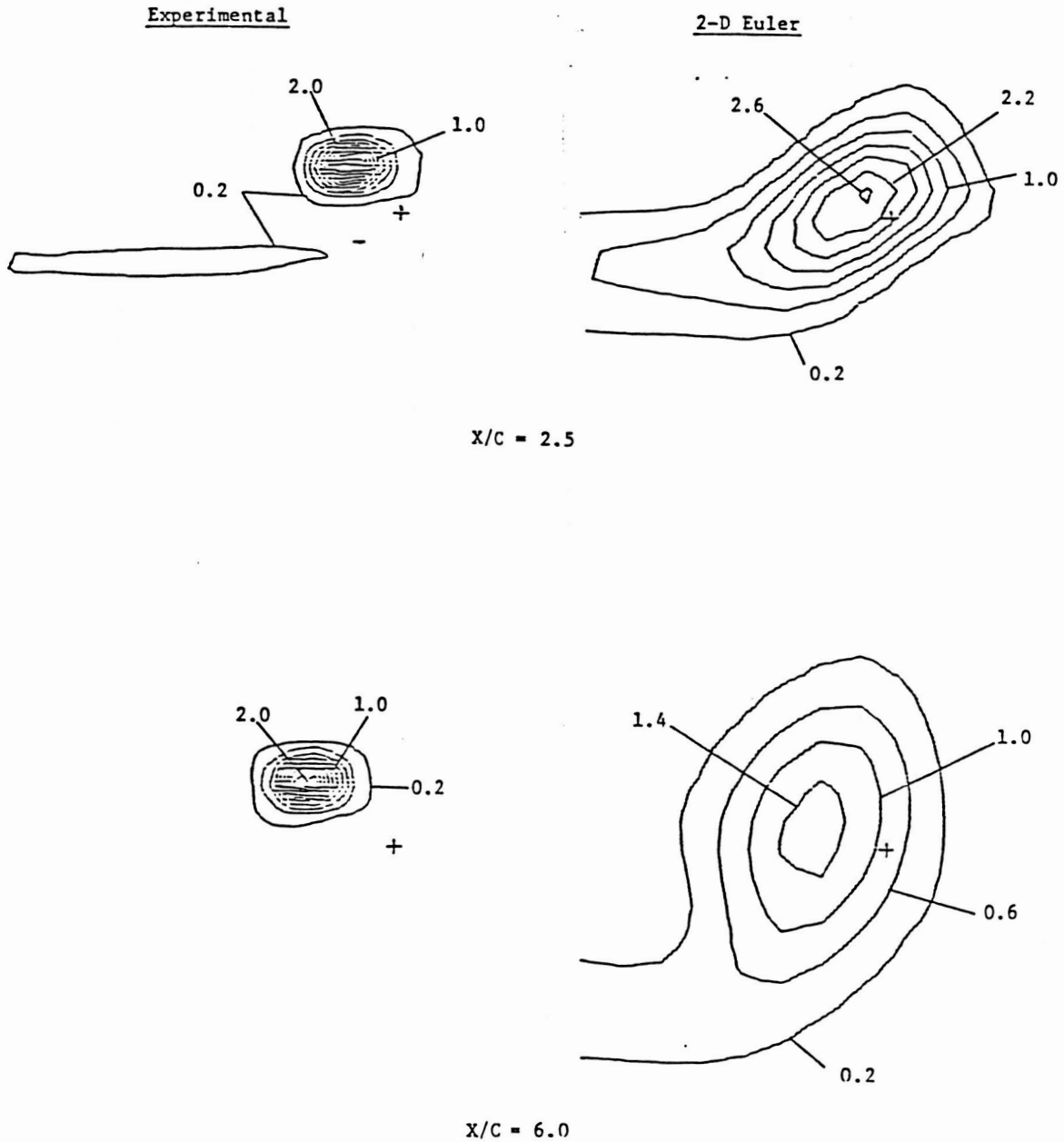


Figure 25 Comparison of vorticity contours to 2-D Euler Method  
 $(\alpha = 8^\circ, Re = 5.30 \times 10^5)$